Desalination 549 (2023) 116322

Contents lists available at ScienceDirect

Desalination

journal homepage: www.elsevier.com/locate/desal

Effluents from the copper electrorefining as a secondary source of antimony: Role of mass transfer on the recovery by electrodeposition

L. Hernández-Pérez, J. Carrillo-Abad, V. Pérez-Herranz, M.T. Montañés, M.C. Martí-Calatayud *

IEC Group, ISIRYM, Universitat Politècnica de València, Camí de Vera s/n, P.O. Box 22012, E-46071, 46022 València, Spain

HIGHLIGHTS

- Antimony is recovered from copper electrorefining effluents.
- Metallic antimony is recovered in spite of the high hydrochloric acid concentration.
- Reduction reactions involved in the system have been studied by voltammetry.
- Electrodeposition of antimony near 100 % is achieved in less than 2 h.
- Improving the hydrodynamic conditions enhances the electrodeposition of antimony.

GRAPHICAL ABSTRACT

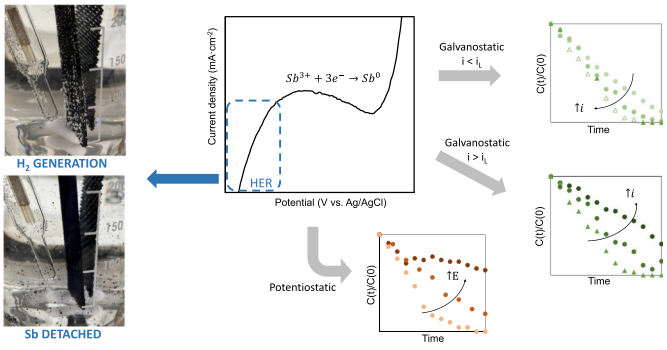

ARTICLE INFO

Keywords:
Industrial wastewater
Antimony recovery
Secondary source
Electrodeposition
Voltammetry

ABSTRACT

The limited availability of antimony has increased the need for exploiting alternative sources to its direct extraction from stibnite deposits. Furthermore, introducing recovery techniques in industries where antimony is released in wastewaters leads to more responsible production routes. In this work, electrodeposition is employed to recover the antimony present in a secondary waste effluent of the copper electrorefining that is highly concentrated in hydrochloric acid. The electrochemical characterization of the system was conducted by voltammetry to identify a range of suitable operating conditions for the potentiostatic and galvanostatic electrorecovery of antimony. In potentiostatic mode, the progress of the secondary electrode reactions of hydrogen and chlorine evolution at potentials more cathodic than −0.38 V vs. Ag/AgCl causes the detachment and redissolution of the deposited antimony. Operating under galvanostatic control, similar effects were observed when the limiting current density is exceeded. Current efficiency and specific energy consumption values above 50 % and below 65 kW·h·kg^{-1}, were achieved below the limiting current density (1.265 mA·cm^{-2}). The operational range where electrodeposition of antimony is accelerated at increasing current densities can be broadened at intensified hydrodynamic conditions and higher concentrations of antimony. The detrimental effect of the hydrogen evolution reaction on the recovery of antimony decreases at high HCl concentrations.

* Corresponding author.
E-mail address: mcmarti@iqn.upv.es (M.C. Martí-Calatayud).

https://doi.org/10.1016/j.desal.2022.116322
Received 1 September 2022; Received in revised form 21 November 2022; Accepted 10 December 2022
Available online 22 December 2022

1. Introduction

In the last years, the scarcity of some raw materials, among them antimony, has been highlighted by different institutions as critical for some industries [1]. Thus, the recovery of such materials from secondary sources has gained attention. Particularly, antimony has several applications in the production of flame retardants, as plastic catalyst, as additive in lubricants and in the manufacture of cable coverings [2,3]. The recovery of antimony from industrial and mine effluents can be seen as a specific milestone in the achievement of the Sustainable Development Goal number 12 of the United Nations (Responsible consumption and production).

The copper production industry generates several waste effluents that contain valuable elements, among them, antimony, bismuth, iron, lead and arsenic [4,5]. Moreover, there is a gradual decrease in ore grades, which implies that the level of these impurities in industrial processes such as copper electrorefining is increasing [6]. Fig. 1 shows one of the final steps in the process of copper production where the sulfuric acid employed in the copper electrorefining is purified and recycled. As shown at the left side of Fig. 1, the sulfuric acid bath is passed through a column with ion exchange resins to separate some of the impurities that were dissolved from the copper anodes during the electrorefining process [6,7]. The resins employed have a strong exchange capacity for multivalent species such as those containing antimony (III) [8]. When the resins become exhausted, they are regenerated by washing with highly concentrated hydrochloric acid. The result of this regeneration is a hydrochloric acid solution with antimony and bismuth, mainly [6]. A further improvement in the copper electrorefining process would be the recovery of Sb present in the regenerating solutions; what would favor the successive reuse of HCl in a closed loop and increase the circularity of the copper industry.

Among the available techniques that could be used to separate Sb from waste effluents, electrochemical deposition stands out on account of its high selectivity. This technique enables the individual recovery of a specific element present in a mixture based on the different reduction potentials of each metal. Taking into account that the solution obtained from the regeneration of the ion exchange resins contains a higher amount of Sb [7], in this work, the recovery of Sb from highly concentrated hydrochloric acid solutions is investigated (right side of Fig. 1).

Several works have focused on recovering metals by means of electrochemical deposition in order to recycle the acidic solution that contains them [9–11]. In the last years, this technique has been employed in the recovery of metals from secondary sources, among them electronic waste [12,13] and wastewater [14,15]. In previous studies, leaching and electrodeposition have been employed as complementary techniques to separate antimony from substrates that contain other metals [16–18]. Most of the works published on the recovery of Sb by means of electrodeposition report significant variations in the efficiency achieved as a function of the applied current density. Awe et al. obtained a current efficiency of 90 % applying a current density of 15 $mA{\cdot}cm^{-2}$ in an effluent containing antimony sulfide, sodium sulfide and sodium hydroxide [19]. In addition, they observed that the current efficiency diminished with the increase in current density. Under optimal conditions, they could recover 74 % of the Sb present in the effluent. Koparal et al. reported a maximum current efficiency of 90 % applying a current density of 5 $mA{\cdot}cm^{-2}$ in an effluent with antimony in sulfuric acid [20]. Moreover, they observed that the current efficiency reached a maximum value at the beginning of the experiment, and it decreased as the Sb became depleted in the solution. With these conditions, they could recover 99.4 % of the Sb present in the effluent. The previous referred studies [19,20], where the electrodeposition of antimony is investigated, are concerned with the determination of the best process operating conditions. However, despite showcasing promising outcomes, most of the results obtained so far are usually not accompanied by a phenomenological interpretation that could shed light on the key factors determining the best conditions for electrodeposition processes.

The aim of this study is the recovery of antimony present in the highly concentrated hydrochloric acid solutions resulting from the regeneration of ion exchange resins (Fig. 1). The electrochemical characterization of the solution has been carried out employing voltammetric measurements, from which the electrode reactions taking place in the system and their related potentials were identified. Moreover, the role of forced convection and the concentration of Sb(III) and HCl on the rate and efficiency of Sb electrodeposition were further investigated. Based on the conditions achieved in the voltammetric study, the

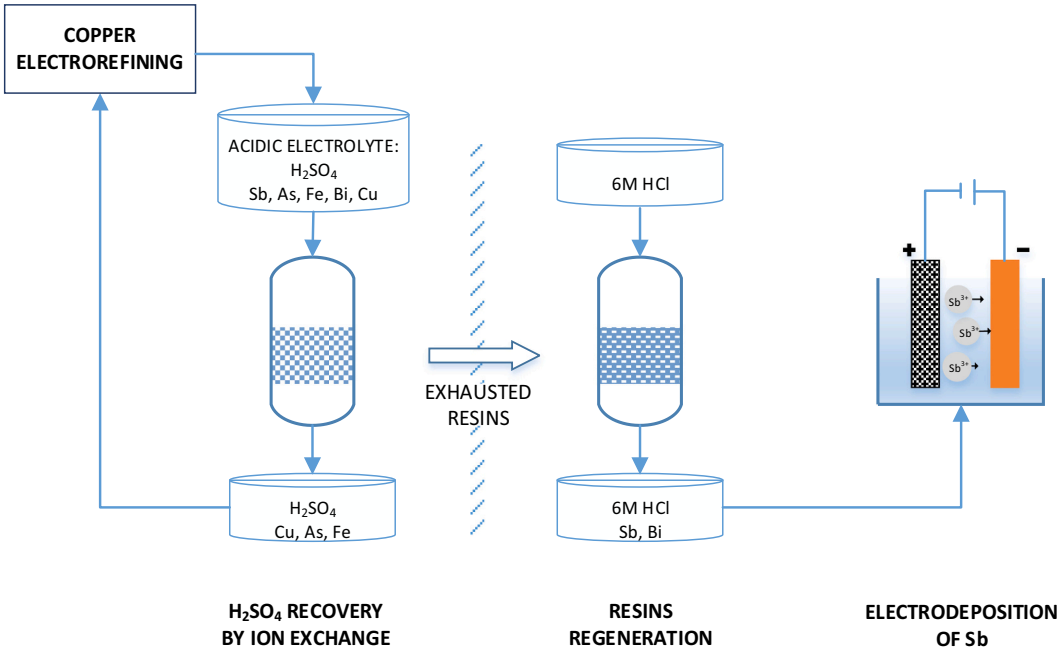

Fig. 1. Steps involved in the recovery of the acidic electrolyte employed in the copper electrorefining, including the recovery of Sb from the regenerating solutions by electrodeposition.

cathodic electrodeposition of antimony was investigated under potentiostatic and galvanostatic conditions.

2. Experimental

2.1. Solutions

The solutions employed in this study emulate the composition in antimony of the spent electrolytes obtained after several steps of regeneration of ion exchange resins [6]. The range of characteristic concentrations of such solutions are: 2–4.5 mM Sb(III) and 1.5–6 M HCl. Note that at this concentration of HCl, antimony is in the solubility range (Fig. S 4, Appendix A). All solutions were prepared using analytical grade reagents, Sb_2O_3 (99 %, Sigma-Aldrich) and HCl (37 %, Panreac), and distilled water (Type 2 water quality according to ASTM D1193-06 standard) with a maximum conductivity of 0.001 mS·cm^{-1}.

2.2. Electrochemical study

Before conducting the electrodeposition experiments, a voltammetric study was carried out to investigate the electrochemical behavior of the system. Cyclic voltammograms and cathodic polarization curves were obtained under varying hydrodynamic conditions.

Cyclic voltammetric tests were conducted employing a conventional three-electrode cell with a rotating disk electrode (RDE). A platinum disc enclosed in Teflon with an effective area of 0.071 cm^2 was employed as working electrode; the reference electrode was a standard Ag/AgCl (3 M KCl) electrode, and the counter electrode was a platinum ring with an area of 1 cm^2. The tests were performed from the open circuit potential (OCP) towards negative potentials at a scan rate of 10 mV·s^{-1}. Various rotation rates of the RDE (500–3500 rpm) were tested and several cycles were executed to stabilize the electrode and to obtain reproducible results.

Cathodic polarization curves were obtained using the electrolysis reactor to be employed in the subsequent electrodeposition experiments (Fig. S 1, Appendix A). It was an undivided reactor composed of a Pyrex glass of 250 mL with three electrodes. The cathode was a copper plate with 40 cm^2 of exposed plating area. A dimensionally stable anode (DSA) electrode composed of a sheet of titanium coated with a mixed metal oxide (RuO_2/IrO_2: 0.70/0.30) with an area of 40 cm^2 acted as the anode and a standard Ag/AgCl (3 M KCl) electrode was used as the reference electrode. A magnetic stirrer with controlled stirring rate (500–950 rpm) was employed during the experiments to adjust the convective regime in the cell. All cathodic polarization curves were obtained between OCP and potentials at which the hydrogen evolution reaction (HER) predominates, at a scan rate of 10 mV·s^{-1}.

2.3. Electrolysis experiments

The electrolysis experiments were carried out under potentiostatic and galvanostatic operation modes in the stirred batch reactor described above. Tests in potentiostatic operation were carried out at different electrode potentials, between −0.34 and −0.65 V vs. Ag/AgCl, which were selected from the polarization curves. The applied currents in galvanostatic operation tests were also selected from the polarization curves. All the experiments were carried out at room temperature using a potentiostat/galvanostat (Autolab PGSTAT 302 N) and NOVA software.

Electrolysis experiments in a two-compartment reactor were executed to evaluate the different reactions taking place in the process. The divided reactor (Fig. S 2, Appendix A) consists of two compartments of 250 mL separated by a cation exchange membrane (Nafion 117, Dupont). The cathodic compartment contains the solution under study and the anodic one contains a solution of 3 M H_2SO_4 (prepared using analytical grade H_2SO_4 96 %, Panreac). The concentration of H_2SO_4 was selected to avoid a significant difference in the osmotic pressure between both compartments.

The duration of the electrodeposition tests was 2 h, and samples were taken from the reactor every 10 min. The cathode potential, current, and cell voltage were recorded during the experiments. The concentration of antimony in the samples was measured by atomic absorption spectroscopy using an atomic absorption spectrometer (Perkin-Elmer model Analyst 100), an antimony hollow cathode lamp at 217.6 nm wavelength, 0.2 nm spectral bandwidth, and a current of 15 mA.

To determine the most favorable conditions for the electrolysis of Sb, the current efficiency (φ) and specific energy consumption (E_s) were analyzed. These parameters are calculated with the following equations [21]:

$$\phi(t) = \frac{n \cdot F \cdot V \cdot (C(0) - C(t))}{\int_0^t I(t)dt} \cdot 100\ (\%) \tag{1}$$

$$E_s(t) = \frac{\int_0^t U(t) \cdot I(t)dt}{M \cdot V \cdot (C(0) - C(t)) \cdot 3600}\ \left(kW \cdot h \cdot kg^{-1}\right) \tag{2}$$

where $C(0)$ and $C(t)$ are the concentration of antimony in the solution (mol·L^{-1}) at the beginning of the tests and at a specific time, respectively; n is the number of electrons exchanged in the metal deposition, in our case $n = 3$; F corresponds to the Faraday constant (96,485.33 C·mol^{-1}); V is the reactor volume (L); $I(t)$ is the function of applied current with time (A); M corresponds to the Sb atomic weight (121.76 g·mol^{-1}); and $U(t)$ is the cell voltage as a function of time (V).

3. Results and discussion

3.1. Electrochemical characterization of the system

The electrodeposition of Sb(III) in the form of metallic Sb in highly concentrated HCl solutions occurs according to the following reaction [22] because the predominant specie in 6 M HCl solutions, is $SbCl_6^{3-}$ (Fig. S 3, Appendix A):

$$SbCl_6^{3-} + 3e^- \rightarrow Sb + 6Cl^- \tag{3}$$

However, in 1.5 M HCl solutions the most concentrated specie is the pentachloride complex, $SbCl_5^{2-}$, (Fig. S 3, Appendix A); so the electrodeposition of Sb(III) in 1.5 M HCl solutions takes place in agreement with the following reaction:

$$SbCl_5^{2-} + 3e^- \rightarrow Sb + 5Cl^- \tag{4}$$

Before conducting the electrodeposition experiments, it is insightful to investigate the process by means of voltammetry. To this aim, the electrochemical behavior of the Sb(III)/Sb system in hydrochloric acid solutions was investigated analyzing the effect of the HCl concentration (Fig. 2a), the Sb concentration (Fig. 2b) and the RDE rotation rate (Fig. 2c) on the voltammograms.

If the voltammograms of Fig. 2a in the forward scan direction are analyzed, one reduction wave can be observed at −0.25 V vs. Ag/AgCl for the 1.5 M HCl solution, and the analogous wave appears at −0.40 V vs. Ag/AgCl for 6 M HCl solutions. The reduction wave is attributed to the electrodeposition of antimony, and it has been detected by other authors in the same range of potentials [23,24]. The HER occurs at potentials more cathodic than the reduction wave, as denoted by the sharp increase in cathodic current (at −0.30 V vs. Ag/AgCl for 1.5 M HCl and −0.50 V vs. Ag/AgCl for 6 M HCl). In the reversed scan, the peak related to the oxidation of metallic Sb to Sb(III) is located at −0.06 V vs. Ag/AgCl for 1.5 M HCl, and at −0.20 V vs. Ag/AgCl for 6 M HCl. Finally, at the anodic edge of the scans, the chlorine evolution reaction starts at +1.10 V vs. Ag/AgCl for 1.5 M HCl, and at +0.98 V vs. Ag/AgCl for 6 M HCl. Regarding the effect of HCl concentration on the Sb electrodeposition, some conclusions can be obtained from the voltammograms. The reduction potential of Sb(III) is displaced to more cathodic values with the increase of the hydrochloric acid concentration. This fact was also

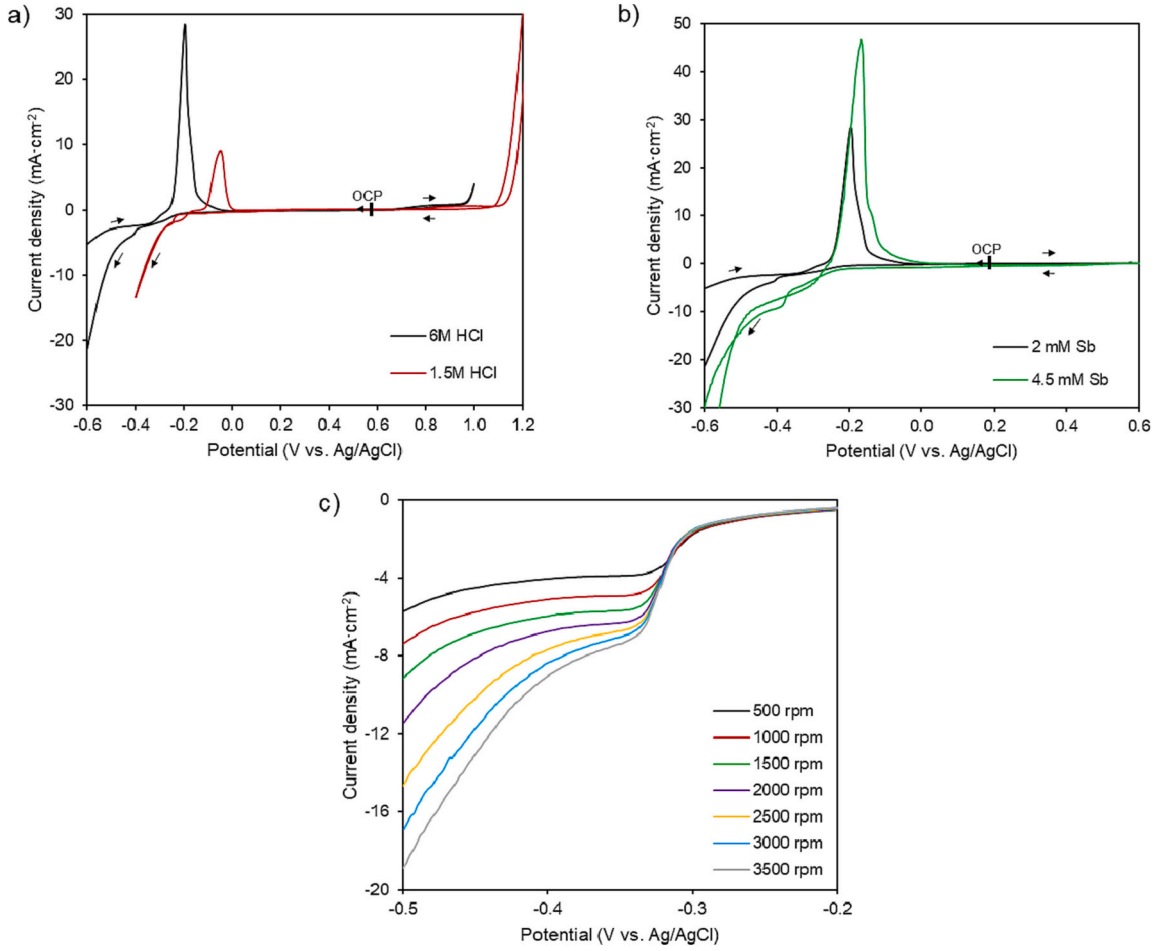

Fig. 2. Cyclic voltammograms obtained at a scan rate of 10 mV·s^{-1}. a) [Sb] = 2 mM, [HCl] = 1.5–6 M. b) [Sb] = 2–4.5 mM, [HCl] = 6 M. c) Linear voltammetric curves obtained at various RDE rotation rates. [Sb] = 4.5 mM, [HCl] = 6 M, scan rate: 10 mV·s^{-1}.

observed by other authors [25] and agrees with the Pourbaix diagrams (Fig. S 3, Appendix A) that show more cathodic potentials for the antimony reduction in the system with a higher HCl concentration. In addition, the current density of the reduction wave rises with increasing the hydrochloric acid concentration. It can be also observed that the corresponding oxidation peak presents a bigger area for 6 M HCl as compared to 1.5 M HCl, revealing that more Sb was electrodeposited during the forward scan (and was liable to be oxidized in the reverse scan). This result indicates that the increase of the hydrochloric acid concentration improves the antimony deposition.

The effect of increasing the Sb concentration on the shape of the voltammogram can be observed in Fig. 2b. The potential of the reduction of Sb(III) to metallic Sb remains constant upon an increase in the Sb concentration, while the current density associated with this peak

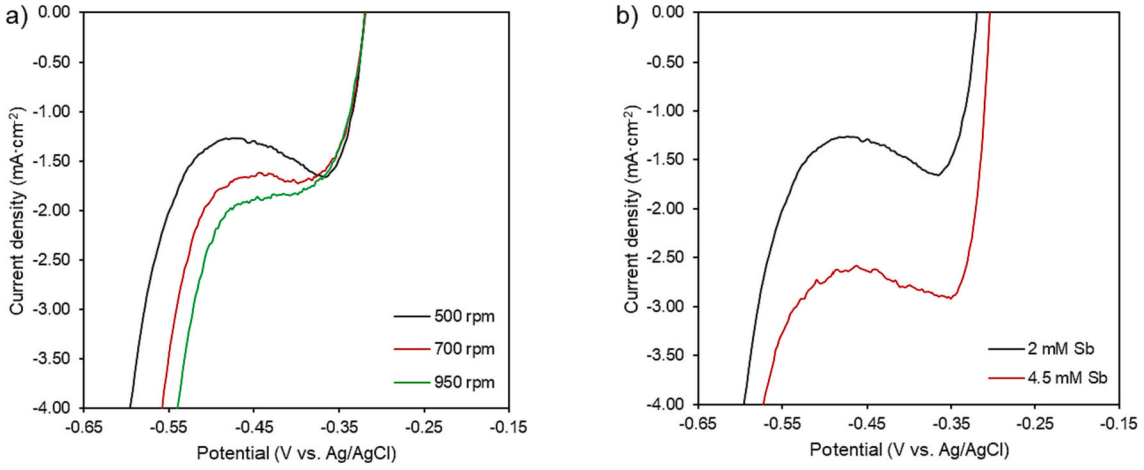

Fig. 3. a) Linear voltammetries registered at various stirring rates. [Sb] = 2 mM, [HCl] = 6 M; b) Linear voltammetries registered at 500 rpm. [Sb] = 2–4.5 mM, [HCl] = 6 M.

increases notably for higher Sb concentrations.

The effect of varying the RDE rotation rate on the reduction of antimony is shown in the linear voltammograms of Fig. 2c. As can be seen in all curves, a diffusion plateau appears between −0.34 and −0.50 V vs. Ag/AgCl approximately, which corresponds to the limiting current density (i_L) and confirms that the reduction of Sb is controlled by mass transfer.

Since mass transfer plays a relevant role in the antimony electrodeposition, the effect of agitation on the linear sweep voltammograms was studied in the same stirred cell and using the Cu electrode with which the subsequent electrolysis experiments were going to be carried out (Fig. 3a). In this set of voltammograms, the influence of Sb concentration on the Sb electrodeposition was also studied (Fig. 3b).

As seen in Fig. 3a, the increase in current density associated with the deposition of Sb appears at electrode potentials close to −0.30 V vs. Ag/AgCl. After the sharp increase of the current density, a plateau is observed at potentials more cathodic than −0.35 V vs. Ag/AgCl. The fact that the i_L values increase with the stirring rate confirms that a higher convective flow improves the delivery of electroactive Sb(III) species from the bulk solution to the electrode surface. Note that the investigated rotation rates correspond to a laminar flow regime, so that this effect can be principally attributed to a thinning of the Diffusion Boundary Layer. At the cathodic end of the plateau region, the current density declines sharply again, which marks the activation of the HER. The convective flow also boosts the HER process, that is, the HER starts at less cathodic potentials when the stirring rate is increased.

Increasing the Sb concentration (Fig. 3b) has a similar effect on the i_L values to that observed when the stirring rate was increased. As expected, larger concentration gradients between the bulk and the electrode surface increase the driving force for the diffusive transport of Sb (III) towards the electrode, and this results in an enhanced electrodeposition process.

3.2. Potentiostatic electrolysis

The evolution of the relative concentration of antimony ($C(t)/C(0)$) during the electrodeposition tests conducted at constant applied potentials for the reference concentration of 2 mM Sb and 6 M HCl and a stirring rate of 500 rpm is shown in Fig. 4. The applied potentials have been selected based on the extension of the plateau registered in the voltammogram of Fig. 3 (curve represented in black in both panels). At −0.34 V vs. Ag/AgCl, where the electrolysis is carried out below the limiting current density, according to the plateau observed in Fig. 3, the relative concentration of Sb decays almost linearly with time, reaching an Sb recovery rate of about 60 % at the end of the electrolysis. At −0.38 V vs. Ag/AgCl, which corresponds to the beginning of the plateau (see Fig. 3), the reactor operates at approximately the limiting current density. Under these conditions, the relative Sb concentration decreases exponentially with time, which is typical of a mass transfer-controlled process [29]. In this case, the almost complete recovery of Sb is achieved at the end of the electrolysis time. At the more cathodic potentials of −0.50 and −0.65 V vs. Ag/AgCl, the reactor operates at (or even above) the limiting current density, but as can be seen in Fig. 4, unlike what might be expected, there is a worsening in the behavior of the system: as the electrode potential becomes more cathodic, the Sb recovery decreases.

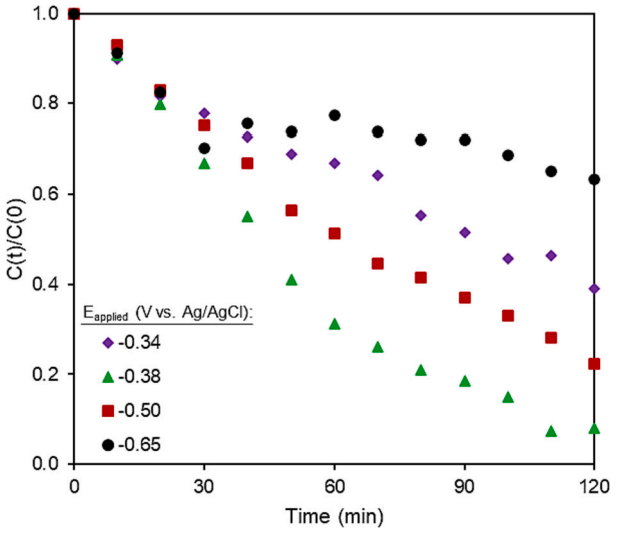

Fig. 4. Evolution of the relative concentration of antimony at different electrode potentials. [Sb] = 2 mM, [HCl] = 6 M, 500 rpm.

This anomalous behavior can be explained on the basis of two different phenomena that undergo in the system, apart from the Sb electrodeposition. The first of such phenomena takes place at the cathode: the generation of hydrogen starts at an electrode potential of −0.50 V vs. Ag/AgCl, while at −0.65 V vs. Ag/AgCl this reaction takes place vigorously, as can be seen in Fig. 3. The HER competes with the electrodeposition of Sb, and the hydrogen formed causes the detachment of the deposited Sb from the electrode into the solution. This behavior is contrary to that observed by other authors, that reported a favored electrodeposition of metals as a consequence of an enhanced mass transfer in the vicinity of the electrode caused by the evolution of gas bubbles [27,30]. Additionally, another reaction taking place on the anode may influence the rate of antimony recovery: the oxidation of chloride ions into chlorine according to:

$$2Cl^- \rightarrow Cl_2(g) + 2e^- \quad (5)$$

Once formed, part of the generated chlorine gas dissolves in water:

$$Cl_2(g) \rightleftharpoons Cl_2(aq) \quad (6)$$

and subsequently, the strongly oxidizing chlorine can dissolve the deposits of antimony that were previously detached from the electrode surface, according to the spontaneous reaction:

$$2Sb + 3Cl_2(aq) \rightarrow 2Sb^{3+} + 6Cl^- \quad (7)$$

The same effect of the dissolution of a deposited metal by the chlorine formed at the anode has been observed by other authors that investigated the electrodeposition of zinc present in hydrochloric acid solutions [31,32]. According to the cyclic voltammograms presented in Fig. 2, while the rate of electrodeposition of Sb is limited by the plateau at i_L, the rates of hydrogen and chlorine generation at the cathode and anode increase without limit at increasing cathodic and anodic potentials, respectively. These reactions are responsible for the corresponding increase in current observed at both ends of the cyclic voltammograms [33].

The varying Sb electrodeposition rates obtained as a function of the applied potential can be further explained by analyzing the evolution of current and current efficiency during the experiments (Figs. S 5 and S 6, Appendix A). Fig. S 5 (Appendix A) shows the evolution of the current with time for the different electrode potentials. For electrode potentials of −0.34 and −0.38 V vs. Ag/AgCl the current initially increases with time, reaches a maximum value at about 80 min of electrolysis and then decreases. The initial increase of current can be explained by the nucleation and growth of the Sb deposit on the copper electrode, what causes an increase in the surface roughness, with the consequent increase in the surface area, and thus, in total current [30,34]. For longer times, the depletion of Sb(III) from the solution involves a decrease in current, since at these potentials, the HER practically does not occur. This evolution results in initial current efficiency values of 100 % at electrode potentials of −0.34 and −0.38 V vs. Ag/AgCl, as can be seen in Fig. S 6 (Appendix A), where the evolution of the current efficiency with time is represented for all electrode potentials.

On the contrary, at the more cathodic potentials of −0.50 and −0.65

V vs. Ag/AgCl, the current increases continuously with time (Fig. S 5, Appendix A). At these potentials, HER takes place from the beginning of the electrolysis, and its contribution to the measured current increases as the concentration of dissolved Sb decreases. Consequently, the higher the current, the higher the hydrogen production at the cathode. In addition to the generation of H_2, in view of the high HCl concentrations studied in the present work, the chlorine production at the anode is not limited by mass transfer. As a result, the current efficiency decreases with time, as seen in Fig. S 6 (Appendix A). It is noteworthy that after 50 min of electrolysis at a potential of −0.65 V vs. Ag/AgCl, the rate of detachment of Sb by the hydrogen formed and its dissolution by chlorine almost equals the rate of electrodeposition, so that the concentration of Sb(III) remains practically constant until the end of the experiment (Fig. 4).

In addition to the experiments carried out, the surface morphology and the composition of the deposits at −0.38 V vs. Ag/AgCl was analyzed using a scanning electron microscope (SEM, ZEISS Ultra 55) and the energy dispersive X-ray analyzer attached to the SEM. A dendritic deposit is observed in the SEM image (Fig. S 7a, Appendix A), and the spectrum obtained confirms the presence of Sb in the deposit (Fig. S 7b, Appendix A).

3.3. Galvanostatic operation

In order to further investigate the mechanism of Sb electrodeposition in HCl solutions, electrolysis tests were performed in galvanostatic mode at various current densities, which were selected from the linear voltammograms shown in Fig. 3. The experiments were carried out at various stirring rates and initial Sb and HCl concentrations, as indicated below in Table 1 and presented in the following subsections.

Fig. 5 shows the evolution of the relative concentration of antimony with time for the reference concentrations of 2 mM Sb(III) and 6 M HCl and a stirring rate of 500 rpm. The applied current densities range between 0.125 and 2.500 mA·cm^{-2}, thus including values below and above the i_L observed in the linear voltammograms of Fig. 3. In a mass transfer-controlled process, the theoretical limiting current density corresponding to the initial electrolyte concentration is given by the following expression (Eq. (8)):

$$i_L(0) = n \cdot F \cdot k_m \cdot C(0) \tag{8}$$

where k_m is the mass transfer coefficient, m·s^{-1}.

As can be seen in Fig. 5, the electrodeposition rate of antimony increases with the applied current density in the range below 1.250 mA·cm^{-2} (Fig. 5a), while it decreases in the range above 1.250 mA·cm^{-2} (Fig. 5b). This behavior, opposed to that observed in other works on the electrodeposition of metals in galvanostatic mode [20,33,35], can be related to the two phenomena mentioned previously. When working at applied current densities lower than the initial limiting current density, $i_L(0)$, the delivery of Sb from the bulk solution to the electrode surface is not limited by diffusion, and HER does not occur significantly. Regarding the rate of chlorine generation at the anode, this is proportional to the low values of applied current density. Consequently, within the range of currents below i_L, the redissolution of Sb should be minimal, and the rate of antimony electrodeposition increases with current. This trend remains until the antimony concentration falls below a value where the electrodeposition process starts to be limited by mass transfer. At higher current densities, the mass transfer limitation is reached earlier and the generation of hydrogen at the cathode and chlorine at the anode become more relevant for the process. Considering the results obtained, for applied current densities higher than 1.250 mA·cm^{-2} (Fig. 5b), the HER rate and the concentration of chlorine may increase with time, eventually causing the partial detachment and redissolution of the deposited Sb. In other words, for applied current densities above the initial limiting current density $i_L(0)$, the antimony deposit detaches due to the generation of hydrogen and can be dissolved due to the action of chlorine (Fig. 5b).

Regarding the trends observed in Fig. 5a, during the first stages of the electrolysis, the relative concentration of antimony decreases linearly with time. This linear decrease can be described by a pseudo zero-order kinetics according to Eq. (9) [35,36]:

$$\frac{C(t)}{C(0)} = 1 - \frac{i \cdot a_e}{n \cdot F \cdot C(0)} t = 1 - \frac{k_0}{C(0)} \cdot t = 1 - k_0' \cdot t \tag{9}$$

where a_e is the electrode specific surface area, defined as the quotient between the electrode area and the reactor volume ($a_e = A/V$), k_0 (mol·L^{-1}·min^{-1}) is the zero-order rate constant for a galvanostatic process, and k_0' (min^{-1}) is the apparent pseudo zero-order rate constant.

In Fig. 5a, the decay of $C(t)/C(0)$ remains linear until mass transfer starts to limit the process and the evolution turns into an exponential decay at the later stages of the electrolysis. Since the limiting current density depends on the electrolyte concentration according to Eq. (8), the decrease of Sb(III) concentration in the bulk solution involves a decrease in the actual limiting current density with time, $i_L(t)$. Eventually, at a specific critical time t_c, the value of $i_L(t_c)$ may reach the same value as the applied current density. From Eq. (8), the concentration of Sb at this moment can be estimated as follows:

$$C(t_c) = \frac{i}{n \cdot F \cdot k_m} \tag{10}$$

While the critical time is given by:

$$t_c = \frac{n \cdot F \cdot k_m \cdot C(0) - i}{i \cdot k_m \cdot a_e} \tag{11}$$

Thus, for low values of current density and at times shorter than t_c, that is, as long as the applied current density is lower than the actual limiting current density, the trend in $C(t)/C(0)$ is linear. However, after

Table 1
Values of the kinetic coefficients and the critical time calculated for the different conditions tested in the electrolytic experiments.

[Sb] (mM)	[HCl] (M)	Stirring rate (rpm)	i (mA·cm^{-2})	k_0' (min^{-1})	t_c (min)	k_1 (min^{-1})	C (t_c) (mM)	R^2
2	6	500	0.125	0.0084	85	0.023	0.080	0.986
			0.625	0.0102	78	0.053	0.328	0.956
			1.250	0.0124	66	0.042	0.832	0.956
			1.875	0.0089				0.985
			2.500	0.0053				0.988
		700	2.500	0.0071				0.975
		950	2.500	0.0107	64	0.024	0.514	0.866
			3.000	0.0140	50	0.010	0.519	0.945
			3.500	0.0089	102	0.096	0.272	0.892
4.5	6	500	1.250	0.0111	55	0.024	0.760	0.921
			1.875	0.0097	64	0.016	0.760	0.783
			2.500	0.0090	81	0.013	0.586	0.997
2	1.5	500	0.125	0.0064				0.980
			0.625	0.0048				0.882

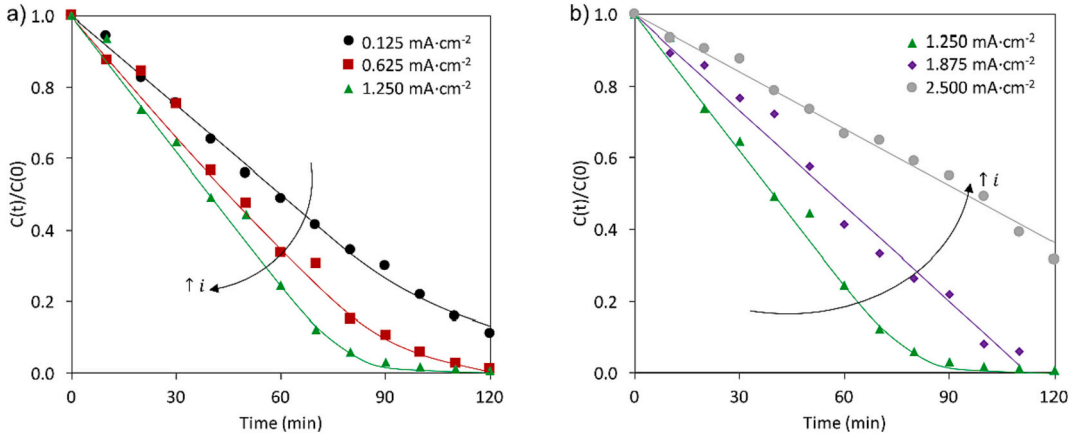

Fig. 5. Evolution of the relative concentration of antimony at different applied current densities. [Sb] = 2 mM, [HCl] = 6 M, 500 rpm. a) 0.125, 0.250, 0.625 and 1.250 mA·cm^{-2}. b) 1.250, 1.875 and 2.500 mA·cm^{-2}.

the critical time, mass transfer becomes the limiting step of the electrodeposition process and $C(t)/C(0)$ starts to decrease exponentially with time according to:

$$\frac{C(t)}{C(0)} = \frac{C(t_c)}{C(0)} \cdot exp(-k_m \cdot a_e \cdot (t - t_c)) = \frac{C(t_c)}{C(0)} \cdot exp(-k_1 \cdot (t - t_c)) \quad (12)$$

Eq. (12) describes a pseudo-first order kinetics corresponding to a mass transfer-limited reaction with a kinetic coefficient, $k_1 = k_m \cdot a_e$.

As can be seen in Fig. 5a, Eq. (9) fits well the experimental data when the applied current density is lower than the $i_L(0)$, while at the latter stages of electrolysis, the evolution of $C(t)/C(0)$ fits well to Eq. (12).

From the non-linear fit of the experimental data to Eqs. (9)–(12) it is possible to determine the values of k_0', k_1, t_c and $C(t_c)$, which are presented in Table 1. Fig. S 8 (Appendix A) shows the variation of k_0' and k_1 with the applied current density for the experiments conducted at $i < i_L(0)$. k_0' increases linearly with the applied current density. This trend has also been observed in electrochemical processes operated in galvanostatic mode which are not limited by mass transfer [37–40]. With respect to k_1, it reaches a maximum value at the current density of 0.625 mA·cm^{-2} and then decreases with the current density. This behavior is in contrast with other studies on electrochemical processes that follow a pseudo-first order kinetics, where a continued increase of k_1 with current density was observed [38,41,42]. The effect of the hydrogen and the chlorine generated on the electrodeposition of antimony may explain this unusual trend, because at 1.250 mA·cm^{-2}, the mass transfer-controlled regime is reached earlier than at 0.625 mA·cm^{-2}, so the HER and the chlorine generation gain more relevance. Regarding the critical time, t_c, it decreases with current density. As expected, the concentration of dissolved Sb in the solution decreases faster at higher current densities, and the process becomes limited by mass transfer earlier. The critical concentration depends on the operating conditions, such as the stirring rate, applied current density and solution characteristics. For tests with 2 mM Sb and 6 M HCl solution at 500 rpm, the critical concentration increases with the applied current density, as can be predicted by Eq. (10) considering the same mass transfer coefficient.

For applied current densities higher than the initial limiting current density ($i > i_L(0)$), an exponential decrease of the relative Sb(III) concentration would be expected. However, as can be seen in Fig. 5b for 1.875 and 2.500 mA·cm^{-2}, the relative concentration of Sb decreases linearly with time. In this case, the value of k_0' (cf. Table 1) decreases with the applied current density as a consequence of the intensified phenomenon of Sb detachment and redissolution discussed above.

According to the results obtained for a stirring rate of 500 rpm and the reference concentrations of 2 mM Sb and 6 M HCl, the expected increase of the Sb recovery rate with current density is limited by the transport of Sb(III) towards the electrode surface. Under a limited supply of Sb to the cathode, the generation of hydrogen becomes more important, and the chlorine generated at the anode may cause the dissolution of detached deposits of Sb. Therefore, an acceleration of the Sb recovery process could be achieved by increasing the range of working current densities below $i_L(0)$; in other words, by increasing $i_L(0)$. According to Eq. (8), this can be achieved by increasing the mass transfer coefficient via improving the hydrodynamic conditions or by increasing the initial concentration of Sb(III). In the following sections, the effect of agitation and Sb(III) concentration on the electrodeposition of Sb at high values of current density is studied.

3.3.1. *Effect of stirring on the electrodeposition*

As discussed previously and already presented in the voltammograms of Fig. 3a, increasing the stirring rate has a positive effect on the limiting current density. This fact can also be deduced from Eq. (8): improving the convective regime in the reactor implies larger mass transfer coefficients and contributes to increase the limiting current density. To confirm that an intensified convection also improves the electrodeposition process, galvanostatic experiments at a high current density and various levels of stirring rate were conducted. Fig. 6 shows the effect of the stirring rate on the evolution of the relative Sb concentration for an applied current density of 2.500 mA·cm^{-2}. With a stirring rate of 500 rpm, this value of current density was high enough to decelerate the electrodeposition of Sb on account of the vigorous HER,

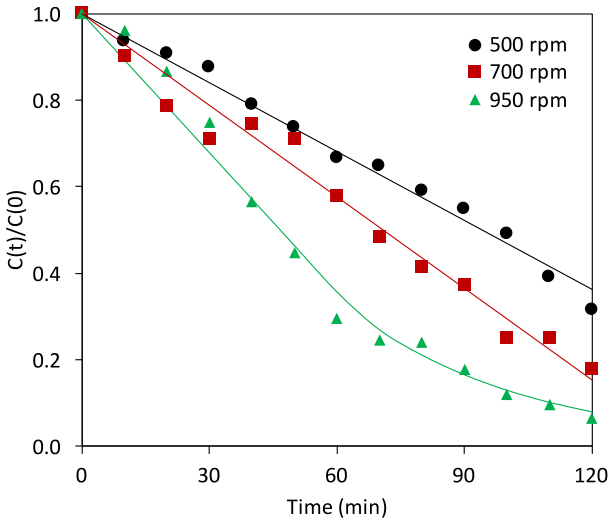

Fig. 6. Evolution of the relative concentration of antimony at 2.500 mA·cm^{-2} and at different stirring rates. [Sb] = 2 mM, [HCl] = 6 M.

as already shown in Fig. 5b. However, the results achieved at 700 and 950 rpm confirm that improving the mass transfer in the reactor has a positive effect on the recovery of antimony. This can be mainly attributed to a decrease in the thickness of the Diffusion Boundary Layer, but probably also to the fact that an increased stirring favors the removal of hydrogen bubbles from the electrode surface.

Despite operating in the regime of currents higher than the limiting value ($i > i_L(0)$), the limiting current density increases with the stirring rate, as seen in Fig. 3a. Consequently, for the same value of applied current density, the $i/i_L(0)$ ratio decreases at intensified convective regimes. This improves the contribution of the Sb electrodeposition to the total cathodic current, while that of the HER can be minimized. As a result, the detachment of Sb deposits by HER is attenuated at higher stirring rates.

Regarding the evolution of the relative Sb concentration with time, the decrease in $C(t)/C(0)$ changes from linear for the stirring rates of 500 and 700 rpm, to a mixed zero and first order kinetics for the highest stirring rate of 950 rpm. In the electrodeposition conducted at 950 rpm, the concentration of Sb has a linear evolution until the critical time is reached, and then the evolution becomes exponential. The kinetic coefficient k_0' increases linearly with the stirring rate, as reported in Table 1 and shown in Fig. S 9, Appendix A.

Fig. 7 shows the effect of the applied current density on the evolution of the relative Sb concentration for the highest stirring rate of 950 rpm. The results are similar to the ones obtained at 500 rpm with lower values of current density (Fig. 5). In these experiments, when the current density increases from 2.5 to 3.0 mA·cm^{-2}, the concentration decays faster, reaching the complete depletion of antimony in the solution. However, if the current density is further increased to 3.5 mA·cm^{-2}, the deposition of antimony becomes decelerated again. Although occurring at a higher level of current densities with a stirring rate of 950 rpm, the HER also turns to be the dominating cathodic process when the amount of supplied Sb(III) from the bulk is not sufficient to react with all the electrons released at the electrode surface. As commented previously, the vigorous generation of hydrogen bubbles induces the detachment of the deposited Sb.

3.3.2. *Effect of Sb concentration on the electrodeposition*

The step of ion-exchange resin regeneration shown in Fig. 1 can lead to variable concentrations of Sb in the problem solutions. According to Eq. (8), and as already proven in Fig. 3b, an increase in the concentration of dissolved Sb in the solutions would result in larger values of i_L, thus broadening the range of currents that could be applied without mass transfer limitations.

Fig. 8 shows the combined effect of stirring rate and Sb concentration on the electrodeposition process for an applied current density of 2.5 mA·cm^{-2}. Taking the system operated at 500 rpm and the concentrations of 2 mM Sb and 6 M HCl as a reference, it can be confirmed that, increasing the concentration of Sb (at a level of 4.5 mM) has a similar positive effect on the Sb recovery as intensifying the convective regime in the reactor (at a level of 950 rpm). Additional tests were performed at the highest level of Sb concentration of 4.5 mM and various current densities. The results obtained with the three applied current densities are very similar (Fig. S 10, Appendix A), which proves that the increased contribution of HER at increasing current densities takes place more gradually for higher Sb(III) concentrations.

3.3.3. *Effect of HCl concentration on the electrodeposition*

The variability in the solution composition can also stem from the choice of HCl concentration used for the regeneration of the ion-exchange beds. In addition to the concentration of 6 M HCl typically used in the process, 1.5 M HCl solutions were studied, since this is the lowest HCl concentration needed to dissolve the Sb(III) present in the resins [7]. In the cyclic voltammograms shown in Fig. 2a, it can be observed that the oxidation peak (corresponding to the reaction Sb to Sb (III)) is bigger with 6 M HCl solutions, corroborating that more Sb(III) was reduced during the forward scan. In addition to this, the onset of the HER is shifted to more cathodic potentials at high HCl concentrations. Therefore, it is also interesting to evaluate which is the effect of the HCl concentration on the Sb electrodeposition process, when this is conducted in galvanostatic experiments of longer duration.

Fig. 9 shows the evolution of antimony concentration for two levels of current density and HCl concentration. Firstly, it can be seen that for a given current density, the concentration of Sb decreases faster with the highest HCl concentration. Regarding the level of current density, it can be observed that with 1.5 M HCl solutions, an increase in current density from 0.125 to 0.625 mA·cm^{-2} results in lower Sb deposition rates. In contrast, for 6 M HCl solutions, the same increase in current density accelerates the electrodeposition process, as expected for the range of currents below $i_L(0)$. These results verify that higher HCl concentrations enhance the Sb deposition and confirm a good agreement with the cyclic voltammetric curves shown in Fig. 2a.

3.3.4. *Effect of Cl_2 formation on the electrodeposition*

The effect of Cl_2 formation on the electrodeposition of antimony has

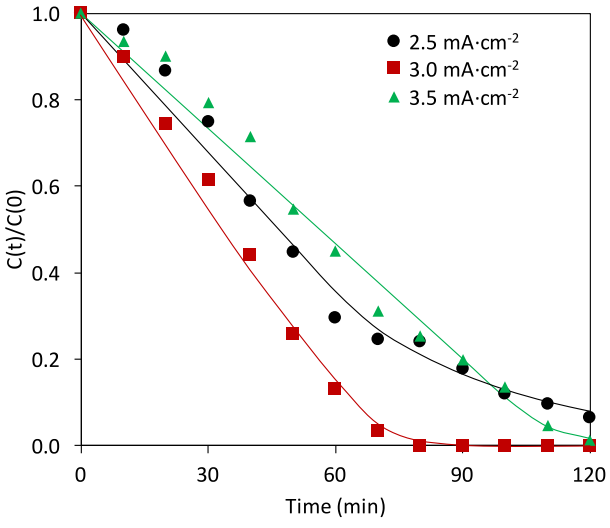

Fig. 7. Evolution of the relative concentration of antimony at different applied current densities. [Sb] = 2 mM, [HCl] = 6 M, 950 rpm.

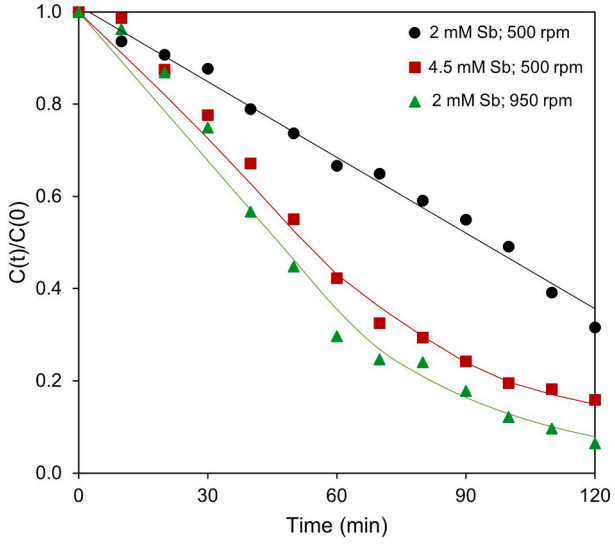

Fig. 8. Evolution of the relative concentration of antimony at 2.5 mA·cm^{-2} and at different stirring rates. [Sb] = 2 and 4.5 mM, [HCl] = 6 M.

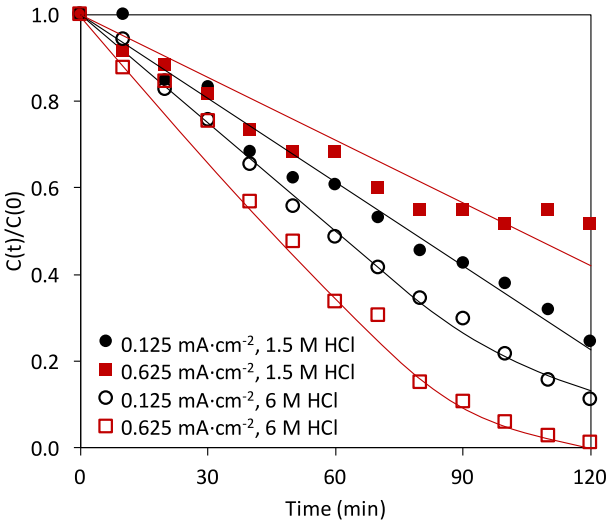

Fig. 9. Evolution of the relative concentration of antimony at different applied current densities and hydrochloric acid concentrations. [Sb] = 2 mM, [HCl] = 1.5–6 M, 500 rpm.

been checked by carrying out various tests in galvanostatic mode using a two-compartment reactor where a cation exchange membrane separates the catholyte and the anolyte. In these experiments, the anolyte was a 3 M H_2SO_4 solution. With this configuration, the chlorine gas evolution happening at the anode is avoided. In Fig. 10, the conversions of Sb, X_{Sb} (Eq. (13)), using both reactors at various applied current densities are compared. At the applied current density of 0.125 mA·cm^{-2}, the best results are obtained with the undivided reactor; this can be explained by the fact that, at low current densities the Cl_2 formation is minimal. At 1.250 mA·cm^{-2}, the total conversion of Sb reached at the end of the experiments is similar using both setups, which also confirms that chlorine gas evolution in the undivided reactor has not affected the amount of antimony deposited. However, at 2.500 mA·cm^{-2}, the percentage of antimony deposited is higher with the two-compartment reactor. This fact demonstrates that chlorine gas evolution affects the antimony deposition with the undivided reactor. However, it can be concluded that the effect of chlorine gas evolution on the antimony deposition is relevant only at the highest applied current densities.

$$X_{Sb}(t) = \frac{C(0) - C(t)}{C(0)} \tag{13}$$

3.3.5. Analysis of the current efficiency and the specific energy consumption

The results presented in previous sections evidence that enhancing the transfer of Sb(III) from the bulk solution towards the electrode is crucial to obtain high Sb recovery rates with shorter times. However, to evaluate if this improvement in the electrodeposition rates at high current densities also involves a more efficient process, it is necessary to evaluate additional indicators. Figs. 11 and 12 show the evolution of current efficiency and specific energy consumption of the galvanostatic electrolysis for the two extreme values of stirring rate: 500 and 950 rpm. Regarding the current efficiency, a decrease of this parameter with the applied current density is observed for the two stirring rates. The same behavior was observed by other authors [19]. This trend can be explained by the larger contribution of the HER to the imposed current, when this is increased and the dissolved Sb reacts faster than it is supplied to the electrode. For the values of current density that are applied at both stirring rates (1.250, 1.875 and 2.500 mA·cm^{-2}), the current efficiency is higher at 950 rpm. This phenomenon is directly related to the increase in the values of $i_L(0)$ as the stirring rate increases. For 950 rpm, the system is operated at lower $i/i_L(0)$ ratios and the HER gains in predominance only at the latter stages of the electrolysis as a consequence of the decrease in Sb concentration.

With respect to the specific energy consumption (Fig. 12), in general, this parameter increases with the current density as a consequence of the increased cell voltage and decreased current efficiency. For the values of current density that are applied at both stirring rates (1.250, 1.875 and 2.500 mA·cm^{-2}), the energy consumption is lower at the highest stirring rate, which confirms that an intensified convective regime improves mass transfer and reduces the level of the HER. Furthermore, by comparing Fig. 12a and b, it can be seen that the minimum energy consumption at 500 rpm is achieved for the lowest current density of 0.125 mA·cm^{-2}. Curiously, a similar value in specific energy consumption can be obtained with the highest stirring rate of 950 rpm at a significantly higher current density of 3 mA·cm^{-2}. Here, it is important to note that the Sb recovery rate is higher at 950 rpm and 3 mA·cm^{-2}, as can be concluded from the evolution of $C(t)/C(0)$ in both cases (compare Figs. 3 and 7), and also from the comparison of the k_0' values shown in Table 1. Therefore, it can be concluded that, by optimizing the

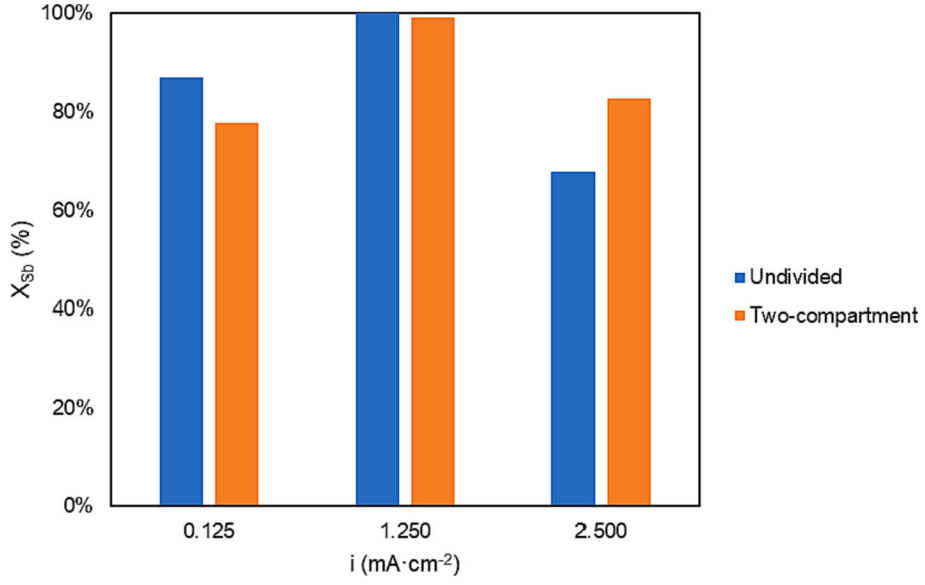

Fig. 10. Final conversion of Sb obtained in the undivided and the two-compartment reactor after 2 h at various applied current densities.

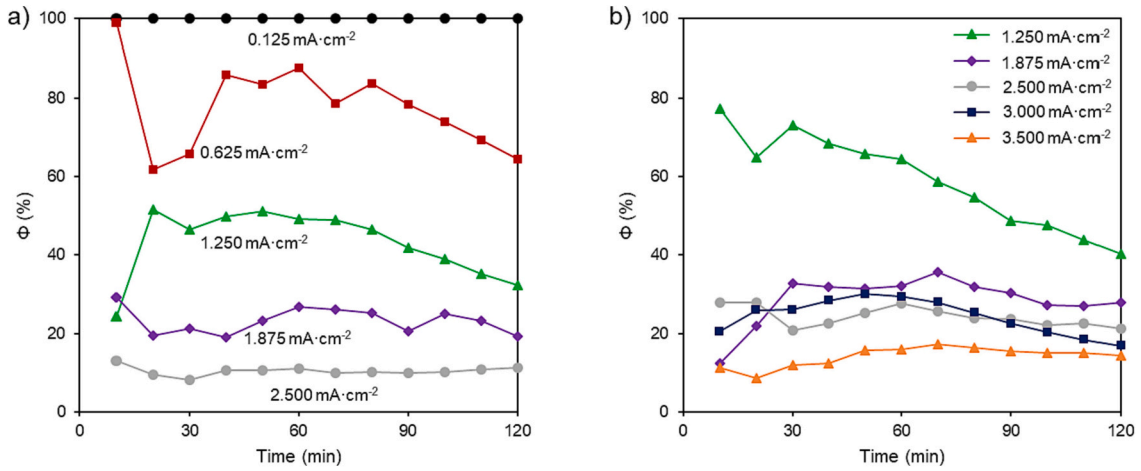

Fig. 11. Evolution of the current efficiency at different applied current: a) at 500 rpm, b) at 950 rpm. [Sb] = 2 mM, [HCl] = 6 M.

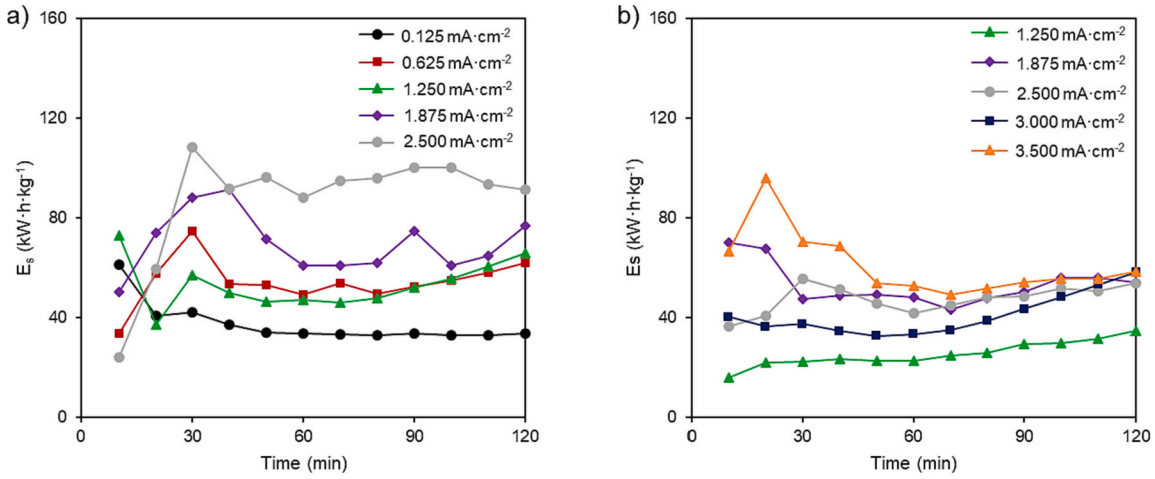

Fig. 12. Evolution of the specific energy consumption at different applied current: a) at 500 rpm, b) at 950 rpm. [Sb] = 2 mM, [HCl] = 6 M.

convective regime, it is possible to recover Sb at a higher rate and with a lower energy consumption.

The trends observed in the figures of merit with the current density and stirring rate confirm the conclusions obtained in Section 3.3.1: the best results of Sb electrodeposition are obtained applying the stirring rate of 950 rpm on account of an improved mass transfer. For the same values of applied current, the current efficiency is higher and the specific energy consumption lower with the highest stirring rate.

4. Conclusions

Antimony is present in secondary waste effluents from the copper electrorefining process. With the aim of recovering the antimony and reusing the HCl used for the regeneration of ion-exchange resins, the electrochemical characterization of the emulated effluent has been carried out, and subsequently, electrodeposition experiments have been executed under various conditions.

The electrochemical characterization by means of voltammetry of the system Sb(III)/Sb in highly concentrated hydrochloric acid leads to the following conclusions:

i) The deposition of Sb(III) in the system of study is a mass transfer-controlled process.
ii) All linear sweep voltammograms show a plateau denoting that the limiting current density for the electrodeposition of Sb is reached. The shape of the plateau depends on the Sb concentration and on the stirring rate. The higher the Sb concentration, the larger the limiting current density; and at increasing stirring rates the limiting current density increases and the length of the plateau decreases.

Electrodeposition experiments confirmed that the amount of Sb recovered diminishes when the applied electrode potentials are more cathodic than −0.38 V vs. Ag/AgCl. This behavior is caused by different phenomena: the HER taking place at the cathode causes the partial detachment of the deposited Sb, and the chlorine generation occurring at the anode can dissolve the metallic antimony that has been detached.

In galvanostatic electrolysis, when the applied current density is lower than the initial limiting current density (1.265 mA·cm^{-2}), the rate of antimony electrodeposition increases with the applied current density. The behavior is the contrary above the initial limiting current density, since the limited supply of dissolved antimony towards the electrode favors the HER. Increasing the Sb recovery rate is achieved by increasing the mass transfer coefficient, either at higher Sb concentrations or with improved hydrodynamic conditions. The detrimental effect of the hydrogen evolution reaction on the recovery of antimony also decreases at high HCl concentrations.

CRediT authorship contribution statement

L. Hernández-Pérez: Investigation, Writing – original draft,

Visualization. **J. Carrillo-Abad:** Methodology, Validation. **V. Pérez-Herranz:** Project administration, Funding acquisition, Writing – review & editing. **M.T. Montañés:** Conceptualization, Supervision, Writing – review & editing. **M.C. Martí-Calatayud:** Conceptualization, Supervision, Writing – review & editing.

Declaration of competing interest

The authors declare that they have no known competing financial interests or personal relationships that could have appeared to influence the work reported in this paper.

Data availability

Data will be made available on request.

Acknowledgments

The authors thank the financial support from the Agencia Estatal de Investigación (AEI/10.13039/501100011033) (Spain) under the project PCI2019-103535 and by FEDER A way of making Europe. Funding for open access charge: CRUE-Universitat Politècnica de València.

Appendix A. Supplementary data

Supplementary data to this article can be found online at https://doi.org/10.1016/j.desal.2022.116322.

References

[1] T. Henckens, Scarce mineral resources: extraction, consumption and limits of sustainability, Resour. Conserv. Recycl. 169 (2021), 105511, https://doi.org/10.1016/J.RESCONREC.2021.105511.
[2] M.L.C.M. Henckens, P.P.J. Driessen, E. Worrell, How can we adapt to geological scarcity of antimony? Investigation of antimony's substitutability and of other measures to achieve a sustainable use, Resour. Conserv. Recycl. 108 (2016) 54–62, https://doi.org/10.1016/j.resconrec.2016.01.012.
[3] H.A. Petersen, T.H.T. Myren, S.J. O'Sullivan, O.R. Luca, Electrochemical methods for materials recycling, Mater. Adv. 2 (2021) 1113–1138, https://doi.org/10.1039/D0MA00689K.
[4] L. Cifuentes, G. Crisóstomo, J.P. Ibez, J.M. Casas, F. Alvarez, G. Cifuentes, On the electrodialysis of aqueous H2SO4-CuSO4 electrolytes with metallic impurities, J. Membr. Sci. 207 (2002) 1–16, https://doi.org/10.1016/S0376-7388(01)00733-5.
[5] T. Oishi, M. Yaguchi, Y. Takai, Hydrometallurgical recovery of high-purity copper cathode from highly impure crude copper, Resour. Conserv. Recycl. 167 (2021), 105382, https://doi.org/10.1016/J.RESCONREC.2020.105382.
[6] K.S. Barros, V.S. Vielmo, B.G. Moreno, G. Riveros, G. Cifuentes, A.M. Bernardes, Chemical composition data of the main stages of copper production from sulfide minerals in Chile: a review to assist circular economy studies, Minerals. 12 (2022), https://doi.org/10.3390/min12020250.
[7] F. Arroyo-Torralvo, A. Rodríguez-Almansa, I. Ruiz, I. González, G. Ríos, C. Fernández-Pereira, L.F. Vilches-Arenas, Optimizing operating conditions in an ion-exchange column treatment applied to the removal of Sb and bi impurities from an electrolyte of a copper electro-refining plant, Hydrometallurgy. 171 (2017) 285–297, https://doi.org/10.1016/j.hydromet.2017.06.009.
[8] J. Li, B.H. Zheng, Y. He, Y. Zhou, X. Chen, S. Ruan, Y. Yang, C. Dai, L. Tang, Antimony contamination, consequences and removal techniques: a review, Ecotoxicol. Environ. Saf. 156 (2018) 125–134, https://doi.org/10.1016/j.ecoenv.2018.03.024.
[9] Y. Yang, C. Lan, Y. Wang, Z. Zhao, B. Li, Recycling of ultrafine NdFeB waste by the selective precipitation of rare earth and the electrodeposition of iron in hydrofluoric acid, Sep. Purif. Technol. 230 (2020), https://doi.org/10.1016/j.seppur.2019.115870.
[10] L. Yang, W. Hu, Z. Chang, T. Liu, D. Fang, P. Shao, H. Shi, X. Luo, Electrochemical recovery and high value-added reutilization of heavy metal ions from wastewater: recent advances and future trends, Environ. Int. 152 (2021), 106512, https://doi.org/10.1016/J.ENVINT.2021.106512.
[11] Y. Liu, Y.Y. Deng, Q. Zhang, H. Liu, Overview of recent developments of resource recovery from wastewater via electrochemistry-based technologies, Sci. Total Environ. 757 (2021), 143901, https://doi.org/10.1016/J.SCITOTENV.2020.143901.
[12] Y. Liu, Q. Song, L. Zhang, Z. Xu, Targeted recovery of ag-pd alloy from polymetallic electronic waste leaching solution via green electrodeposition technology and its mechanism, Sep. Purif. Technol. 280 (2022) 1383–5866, https://doi.org/10.1016/J.SEPPUR.2021.118944.
[13] Y. Liu, Q. Song, L. Zhang, Z. Xu, Separation of metals from Ni-Cu-Ag-Pd-Bi-Sn multi-metal system of e-waste by leaching and stepwise potential-controlled electrodeposition, J. Hazard. Mater. 408 (2021), 124772, https://doi.org/10.1016/J.JHAZMAT.2020.124772.
[14] C. Wu, J. Gao, Y. Liu, W. Jiao, G. Su, R. Zheng, H. Zhong, High-gravity intensified electrodeposition for efficient removal of Cd2+ from heavy metal wastewater, Sep. Purif. Technol. 289 (2022), 120809, https://doi.org/10.1016/j.seppur.2022.120809.
[15] J. Nan Gu, J. Liang, C. Chen, K. Li, W. Zhou, J. Jia, T. Sun, Treatment of real deplating wastewater through an environmental friendly precipitation-electrodeposition-oxidation process: Recovery of silver and copper and reuse of wastewater, Sep. Purif. Technol. 248 (2020), https://doi.org/10.1016/J.SEPPUR.2020.117082.
[16] J.A. Barragan, C. Ponce De León, J.R. Alemán Castro, A. Peregrina-Lucano, F. Gómez-Zamudio, E.R. Larios-Durán, Copper and antimony recovery from electronic waste by hydrometallurgical and electrochemical techniques, ACS, Omega 5 (2020) 12355–12363, https://doi.org/10.1021/acsomega.0c01100.
[17] D. Dupont, S. Arnout, P.T. Jones, K. Binnemans, Antimony recovery from end-of-life products and industrial process residues: a critical review, J. Sustain. Metall. 2 (2016) 79–103, https://doi.org/10.1007/s40831-016-0043-y.
[18] J.G. Yang, Y.T. Wu, A hydrometallurgical process for the separation and recovery of antimony, Hydrometallurgy 143 (2014) 68–74, https://doi.org/10.1016/j.hydromet.2014.01.002.
[19] S.A. Awe, J.E. Sundkvist, N.J. Bolin, Å. Sandström, Process flowsheet development for recovering antimony from Sb-bearing copper concentrates, Miner. Eng. 49 (2013) 45–53, https://doi.org/10.1016/j.mineng.2013.04.026.
[20] S.S. Koparal, R. Özgür, Ü.B. Öğütveren, H. Bergmann, Antimony removal from model acid solutions by electrodeposition, Sep. Purif. Technol. 37 (2004) 107–116, https://doi.org/10.1016/j.seppur.2003.09.001.
[21] J. Carrillo-Abad, M. García-Gabaldón, V. Pérez-Herranz, pH effect on zinc recovery from the spent pickling baths of hot dip galvanizing industries, Sep. Purif. Technol. 177 (2017) 21–28, https://doi.org/10.1016/j.seppur.2016.12.034.
[22] G. Senanayake, D.M. Muir, Speciation and reduction potentials of metal ions in concentrated chloride and sulfate solutions relevant to processing base metal sulfides, Metall. Trans. B 19 (1988) 37–45, https://doi.org/10.1007/BF02666488.
[23] H. Ebe, M. Ueda, T. Ohtsuka, Electrodeposition of Sb, Bi, Te, and their alloys in AlCl3-NaCl-KCl molten salt, Electrochim. Acta 53 (2007) 100–105, https://doi.org/10.1016/j.electacta.2007.03.017.
[24] Y. Lin, P. Ning, Y. Cui, C. Zhang, M. Xu, P. Dong, Z. Zhou, Y. Zhang, Electrodeposition behaviour of antimony in H2SO4-NH4F-SbF3 solutions, Int. J. Electrochem. Sci. 14 (2019) 4003–4019, https://doi.org/10.20964/2019.03.33.
[25] H. Verplaetse, P. Kiekens, E. Temmerman, F. Verbeek, Catalytic influence of Cl-, Br-, I- and SCN- on the cyclic voltammetric behaviour of Sb(III), Talanta 28 (1981) 431–435, https://doi.org/10.1016/0039-9140(81)80063-X.
[27] A.C. Kasper, H.M. Veit, M. García-Gabaldón, V.P. Herranz, Electrochemical study of gold recovery from ammoniacal thiosulfate, simulating the PCBs leaching of mobile phones, Electrochim. Acta 259 (2018) 500–509, https://doi.org/10.1016/j.electacta.2017.10.161.
[29] M.C. Martí-Calatayud, E. Dionís, S. Mestre, V. Pérez-Herranz, Antimony-doped tin dioxide ceramics used as standalone membrane electrodes in electrofiltration reactors enhance the oxidation of organic micropollutants, J. Clean. Prod. 363 (2022), 132342, https://doi.org/10.1016/J.JCLEPRO.2022.132342.
[30] M. García-Gabaldón, V. Pérez-Herranz, J. García-Antón, J.L. Guiñón, Electrochemical recovery of tin and palladium from the activating solutions of the electroless plating of polymers: potentiostatic operation, Sep. Purif. Technol. 45 (2005) 183–191, https://doi.org/10.1016/J.SEPPUR.2005.03.008.
[31] J. Carrillo-Abad, M. García-Gabaldón, E. Ortega, V. Pérez-Herranz, Electrochemical recovery of zinc from the spent pickling baths coming from the hot dip galvanizing industry. Potentiostatic operation, Sep. Purif. Technol. 81 (2011) 200–207, https://doi.org/10.1016/j.seppur.2011.07.029.
[32] J. Carrillo-Abad, M. García-Gabaldón, V. Pérez-Herranz, Treatment of spent pickling baths coming from hot dip galvanizing by means of an electrochemical membrane reactor, Desalination 343 (2014) 38–47, https://doi.org/10.1016/J.DESAL.2013.11.040.
[33] V.R.C. Thanu, M. Jayakumar, Electrochemical recovery of antimony and bismuth from spent electrolytes, Sep. Purif. Technol. 235 (2020), 116169, https://doi.org/10.1016/j.seppur.2019.116169.
[34] J.C. Bazan, J.M. Bisang, Electrochemical removal of tin from dilute aqueous sulfate solutions using a rotating cylinder electrode of expanded metal, J. Appl. Electrochem. 34 (2004) 501–506, https://doi.org/10.1023/B:JACH.0000021894.86112.63.
[35] J. Carrillo-Abad, M. García-Gabaldón, E. Ortega, V. Pérez-Herranz, Recovery of zinc from spent pickling solutions using an electrochemical reactor in presence and absence of an anion-exchange membrane: galvanostatic operation, Sep. Purif. Technol. 98 (2012) 366–374, https://doi.org/10.1016/J.SEPPUR.2012.08.006.
[36] J. Carrillo-Abad, M. García-Gabaldón, V. Pérez-Herranz, Electrochemical recovery of zinc from the spent pickling solutions coming from hot dip galvanizing industries. Galvanostatic operation, Int. J. Electrochem. Sci. 7 (2012) 5442–5456 (accessed September 2, 2021), www.electrochemsci.org.
[37] L. Xu, S. Tang, K. Wang, X. Ma, J. Niu, Insights into the degradation and detoxication mechanisms of aqueous capecitabine in electrochemical oxidation process, Chemosphere 241 (2020), https://doi.org/10.1016/j.chemosphere.2019.125058.
[38] B.N. Grgur, D.Ž. Mijin, A kinetics study of the methomyl electrochemical degradation in the chloride containing solutions, Appl. Catal. B Environ. 147 (2014) 429–438, https://doi.org/10.1016/j.apcatb.2013.09.028.

[39] E. Hmani, Y. Samet, R. Abdelhédi, Electrochemical degradation of auramine-O dye at boron-doped diamond and lead dioxide electrodes, Diam. Relat. Mater. 30 (2012) 1–8, https://doi.org/10.1016/j.diamond.2012.08.003.
[40] J. Zambrano, B. Min, Electrochemical treatment of leachate containing highly concentrated phenol and ammonia using a Pt/Ti anode at different current densities, Environ. Technol. Innov. 18 (2020), 100632, https://doi.org/10.1016/J.ETI.2020.100632.
[41] Y. Samet, L. Agengui, R. Abdelhédi, Electrochemical degradation of chlorpyrifos pesticide in aqueous solutions by anodic oxidation at boron-doped diamond electrodes, Chem. Eng. J. 161 (2010) 167–172, https://doi.org/10.1016/j.cej.2010.04.060.
[42] F. Escalona-Durán, D. Ribeiro da Silva, C.A. Martínez-Huitle, P. Villegas-Guzman, The synergic persulfate-sodium dodecyl sulfate effect during the electro-oxidation of caffeine using active and non-active anodes, Chemosphere 253 (2020), 126599, https://doi.org/10.1016/j.chemosphere.2020.126599.